



HAL
open science

Permeability changes in coal seams: the role of anisotropy

L.L. Wang, Matthieu Vandamme, Jean-Michel Pereira, Patrick Dangla,
Nicolas Espinoza

► **To cite this version:**

L.L. Wang, Matthieu Vandamme, Jean-Michel Pereira, Patrick Dangla, Nicolas Espinoza. Permeability changes in coal seams: the role of anisotropy. *International Journal of Coal Geology*, 2018, 199, pp.52-64. 10.1016/j.coal.2018.09.014 . hal-02125805

HAL Id: hal-02125805

<https://enpc.hal.science/hal-02125805>

Submitted on 10 May 2019

HAL is a multi-disciplinary open access archive for the deposit and dissemination of scientific research documents, whether they are published or not. The documents may come from teaching and research institutions in France or abroad, or from public or private research centers.

L'archive ouverte pluridisciplinaire **HAL**, est destinée au dépôt et à la diffusion de documents scientifiques de niveau recherche, publiés ou non, émanant des établissements d'enseignement et de recherche français ou étrangers, des laboratoires publics ou privés.

Permeability changes in coal seams: the role of anisotropy

L.L.Wang^{a,*}, M.Vandamme^a, J.M.Pereira^a, P.Dangla^a, N.Espinoza^b

^a*Laboratoire Navier, Université Paris-Est, École des Ponts ParisTech,
77455 Marne-la-Vallée Cedex, France*

^b*Department of Petroleum and Geosystems Engineering, The University of Texas at Austin, United States*

Abstract

The permeability of coal seams is pore pressure-dependent. A number of analytical models have been proposed to investigate this problem, but many disregard a crucial factor: the anisotropy of coal. This paper is devoted to investigating the role of anisotropy in modeling the change of horizontal permeability with pressure. Analysis is conducted using a fully anisotropic model that incorporates both the anisotropies of mechanical properties and of the permeability dependence on stresses. Analytical expressions of the pressure-permeability relationship are derived in oedometric and isochoric geomechanical conditions, and validations are conducted against both laboratory and field data. Then, the roles of the anisotropy of stiffness and of permeability dependence on stresses in the permeability-change model are explored. We demonstrate that the mechanical anisotropy can be simplified to an isotropic model without introducing significant errors in prediction of pressure-permeability relationship, while neglecting the anisotropy of permeability dependence on stresses leads to considerable errors. When both anisotropy sources are disregarded, the pressure-permeability curve can be exactly reproduced by a totally isotropic material in both oedometric and isotropic conditions. However, the material properties (e.g., bulk modulus) are skewed; moreover, such an equivalent material might lead to significant errors in other geomechanical conditions. Finally, the permeability change is investigated at the reservoir scale, and the reservoir simulation results confirm the conclusions obtained from the analytical analysis.

Keywords: Coalbed methane, permeability, anisotropy, analytical modeling, reservoir simulation

1. Introduction

Coalbed methane (CBM) is an important source of energy in the United States, Canada, Australia, and China among other countries. Different from other geomaterials encountered in natural gas recovery,

*Corresponding author, now at China University of Petroleum, Beijing
Email addresses: linlin.wang@cup.edu.cn (L.L.Wang), matthieu.vandamme@enpc.fr (M.Vandamme),
jeanmichel.pereira@enpc.fr (J.M.Pereira), patrick.dangla@ifffstar.fr (P.Dangla), espinoza@austin.utexas.edu (N.Espinoza)

60
61
62
63
64
65 coalbeds are conferred unique poromechanical properties by their two-scale porosity systems: macro-porosity
66 and micro-porosity (Espinoza et al., 2014; Nikoosokhan et al., 2014). The macro-pores in coalbeds are
67 commonly constituted by cleats, that are, natural fractures developed during diagenetic processes (Laubach
68 et al., 1998). The cleats act as the major channel for methane to flow and thus govern the permeability of
69 fractured coal seams. Between cleats, one finds a microporous organic continuum, routinely called as coal
70 matrix. Methane is stored inside the micro-pores of coal matrix. In the micro-pores (typically sized in the
71 order of 10^{-9} to 10^{-8} m), all fluid molecules interact with the atoms of solid matrix; they are therefore not
72 in their bulk state as in the macro-pores but are in adsorbed state (Vandamme et al., 2010; Brochard et al.,
73 2012). The adsorbed state of methane in micro-pores governs the adsorption/desorption phenomena and
74 subsequent swelling/shrinking of coal matrix (Pan and Connell, 2007; Day et al., 2008).

75
76
77
78
79
80
81 The permeability of fractured CBM reservoirs changes with depletion during production, and this process
82 plays an important role during production and enhanced recovery operations. The permeability change with
83 depletion (i.e., decrease of pore pressure) mainly stems from two mechanisms with opposing effects. The
84 first mechanism involves the mechanical deformation due to pressure changes: with decreasing pressure, an
85 increase in effective stress leads to compression of coal and reduction in cleat porosity, so the permeability
86 decreases. The second mechanism is desorption-induced shrinkage of the coal matrix with depletion, resulting
87 in an increase in cleat aperture and thus a rise in permeability.

88
89
90
91 Several analytical models of pressure-dependent permeability have been proposed such as P-M model
92 (Palmer and Mansoori, 1998; Palmer et al., 2007), S-D model (Shi and Durucan, 2004), C-B model (Cui and
93 Bustin, 2005; Cui et al., 2007). A detailed review of these models can be found in Shi and Durucan (2004);
94 Connell (2009); Palmer (2009). These models can be broadly classified into two categories: strain-based
95 and stress-based. The strain-based models relate the permeability (k) to the cleat porosity (ϕ_c) using the
96 bundled-matchstick conceptual model (Seidle et al., 1992), e.g.: $k/k_0 = (\phi_c/\phi_{c0})^3$, where the subscript 0
97 refers to a reference state. For the stress-based models, the permeability is related to effective stress, σ' ,
98 e.g.: $k/k_0 = e^{-3\alpha(\sigma' - \sigma'_0)}$, where α is cleat (volume) compressibility. These models are supported by a wide
99 variety of experimental measurements and have been useful for history-matching various CBM plays. In
100 modeling the permeability evolution, the anisotropy of coal is a crucial influencing factor. This factor has
101 been investigated (Day et al., 2008; Wang et al., 2009; Pan and Connell, 2011; Wang et al., 2013, 2014) but
102 needs to be further explored.

103
104
105
106
107
108
109
110 Considering the stress-based models, anisotropy exists in two aspects: the mechanical behaviour (to
111 compute the effective stress) and the permeability dependence on stresses (related to cleat compressibil-

119
120
121
122
123
124 ity). As most geomaterials, coal seams exhibit transverse isotropy of its mechanical behaviour. Because
125 of the dual-porosity system, the mechanical anisotropy of coal seams is controlled by two opposite effects.
126 Regarding the coal matrix, the lamination and preferred orientation of the macerals during sedimentation,
127 compaction and diagenesis processes contribute to an intrinsic anisotropy of the coal matrix: the horizontal
128 Young's modulus is greater than the vertical one, $E/E_3 > 1$ (the axis 3 is vertical). Thus, this intrinsic
129 anisotropy increases with the degree of maturation, as demonstrated by Morcote et al. (2010). Regarding the
130 cleats, they are prone to be sub-vertically oriented and thus counteract the effect of bedding. In theory, the
131 compressibility of vertical cleats can lead E/E_3 at the seam scale to be less than 1. The cleats are sensitive
132 to the confining stress: sealing the vertical cleats leads the anisotropy to be more and more dominated by
133 the fabric and so causes E/E_3 to increase. Combining the two opposite effects, the anisotropy of elastic
134 properties of coal seams is variable, depending on the degree of maturation, on the confining stress, and on
135 the size of tested samples (number of cleats). For instance, the ultrasonic velocity measurements by Morcote
136 et al. (2010) revealed that horizontal P-wave velocities are greater than vertical velocities for three types
137 of coal. Espinoza et al. (2014); Hol and Spiers (2012) found E and E_3 are comparable. However, Pone et
138 al. (2010) showed that, for a coal sample exposed to 6.9 MPa hydrostatic stress, the y -axis strain is greater
139 than the z -axis strain (z -axis is the vertical direction). Beside the mechanical anisotropy, how permeability
140 depends on effective stresses is also anisotropic. As shown by Espinoza et al. (2014), variation of horizontal
141 effective stress leads to more change in horizontal permeability compared to variation of vertical effective
142 stress with the same magnitude, indicating the anisotropy of the cleat compressibility α .

143
144
145
146
147
148
149 This paper is devoted to investigating the role of anisotropy in the permeability changes in coal seams.
150 It should be noted that the permeability of coal seams is anisotropic: the horizontal permeability is different
151 from the vertical one. However, the present work focuses on the horizontal permeability only. This is
152 because CBM formations are commonly thin, and hence mostly horizontal flow is involved in the production
153 of methane. Therefore, for what concerns CBM processes, the horizontal permeability predominates, and the
154 role of the vertical permeability is secondary. In this sense, the term "permeability" used in the present work
155 specifically refers to the horizontal permeability. In summary, the paper focuses on the role of anisotropies
156 (i.e., anisotropy of the mechanical properties and anisotropy of the dependence of permeability on stresses)
157 in the change of the horizontal permeability, not on the anisotropy of permeability itself. The paper is
158 composed of four parts. After the introduction, the theoretical background used for the analysis is shortly
159 recalled, including a transverse isotropic poromechanical model and a permeability law that depends in a
160 transversely isotropic manner on effective stresses. Then, the role of anisotropy is investigated by analytical
161
162
163
164
165
166
167
168
169
170
171

178 modeling at the scale of a representative element volume (REV) as well as numerical modeling at the scale
 179 of a CBM reservoir.
 180
 181
 182

183 2. Theory

184 2.1. Transverse isotropic poromechanical model

185 The poromechanical model used in this work is a double porosity transverse isotropic model developed
 186 by Espinoza et al. (2014). In brief, the model for coal seams is based on poromechanical equations that
 187 explicitly take into account the effect of adsorption on the mechanical behavior of a microporous medium
 188 (Brochard et al., 2012). As discussed previously, the double porosity system of coal seams is composed
 189 of 1) the cleat macro-porosity where the fluid is in bulk state, and 2) the micro-porosity within the coal
 190 matrix where the fluid is in adsorbed state, and where adsorptive-mechanical couplings (e.g., swelling or
 191 shrinking) originate. The contribution of cleat compressibility to the poromechanical behaviour of coal seams
 192 is modelled using conventional anisotropic poroelasticity (Cheng, 1997); the effect of adsorption-induced
 193 phenomena in the coal matrix is modelled using the theory of generalized poromechanics for microporous
 194 media developed by Brochard et al. (2012) and Espinoza et al. (2013). The model equations are established
 195 from a thermodynamical formulation on the basis of energy conservation. Details about the model derivation
 196 can be found in Espinoza et al. (2014), and a more detailed formulation for isotropic solids can be found in
 197 Nikoosokhan et al. (2014). We merely recall the model equations (the symmetry is around axis 3):
 198
 199
 200
 201
 202
 203
 204
 205
 206
 207
 208
 209
 210
 211

$$\begin{cases}
 \Delta\sigma_{11} = C_{11}\Delta\varepsilon_{11} + C_{12}\Delta\varepsilon_{22} + C_{13}\Delta\varepsilon_{33} - b_1\Delta P_c - (1 - b_1)\Delta S^a(P_m) \\
 \Delta\sigma_{22} = C_{12}\Delta\varepsilon_{11} + C_{11}\Delta\varepsilon_{22} + C_{13}\Delta\varepsilon_{33} - b_1\Delta P_c - (1 - b_1)\Delta S^a(P_m) \\
 \Delta\sigma_{33} = C_{13}\Delta\varepsilon_{11} + C_{13}\Delta\varepsilon_{22} + C_{33}\Delta\varepsilon_{33} - b_3\Delta P_c - (1 - b_3)\Delta S^a(P_m) \\
 \Delta\sigma_{23} = 2C_{44}\Delta\varepsilon_{23} \\
 \Delta\sigma_{31} = 2C_{44}\Delta\varepsilon_{31} \\
 \Delta\sigma_{12} = (C_{11} - C_{12})\Delta\varepsilon_{12} \\
 \Delta\phi_c = b_1(\Delta\varepsilon_{11} + \Delta\varepsilon_{22}) + b_3\Delta\varepsilon_{33} + [\Delta P_c - \Delta S^a(P_m)]/N \\
 n_T = (1 - \phi_{c0})n_m(P_m, \varepsilon_m) + \rho_b\phi_c
 \end{cases} \quad (1)$$

212 The first seven equations are the conventional anisotropic poroelasticity added with a term S_a . σ_{ij}
 213 and ε_{ij} are total stress and strain tensors defined at the coal seam scale; P_c is the pressure of fluid in the
 214 cleat. C_{11} , C_{12} , C_{13} , C_{33} , C_{44} are the five independent stiffness coefficients; b_1 and b_3 are cleat-induced
 215
 216
 217
 218
 219
 220
 221
 222
 223
 224
 225
 226

237
 238
 239
 240
 241
 242 Biot coefficients; N is Biot modulus; ϕ_c is cleat porosity. The term S_a quantifies the stress needed to keep
 243 the coal matrix at zero volumetric strain during adsorption (see the first three equations), so it is termed
 244 adsorption stress. The last eighth equation describes the total amount of fluid in per unit volume of coal
 245 seam, n_T , as the sum of two terms: 1) the amount of fluid adsorbed in the matrix, n_m , and 2) the amount
 246 of fluid in the cleats, which is equal to the cleat porosity, ϕ_c , multiplied by the bulk fluid molar density, ρ_b .
 247 The coal matrix strain ε_m is related to the volumetric strain at the coal seam REV scale $\varepsilon = \varepsilon_{11} + \varepsilon_{22} + \varepsilon_{33}$
 248 through the following relation (Coussy, 2010):
 249
 250
 251
 252

$$253 \varepsilon_m = \frac{\varepsilon - (\phi_c - \phi_{c0})}{1 - \phi_{c0}} \quad (2)$$

254 where ϕ_{c0} is the reference porosity of an undeformed fractured coal. The adsorbed fluid in the coal matrix,
 255 n_m , depends both on fluid pressure, P_m , and on volumetric strain, ε_m . Since strains of the coal matrix are
 256 small, the amount n_m of adsorbed fluid can be approximated by its first-order expression with respect to
 257 ε_m (Brochard et al., 2012):
 258
 259
 260
 261
 262

$$263 n_m(P_m, \varepsilon_m) = n_{m0}(P_m) [1 + c(P_m) \varepsilon_m] \quad (3)$$

264 where n_{m0} is the adsorbed quantity at zero matrix strain. The adsorption isotherm is written here in form
 265 of Langmuir equation $n_{m0} = n_0^{\max} P_m / (P_L + P_m)$, where n_0^{\max} and P_L are two constants. The term $c(P_m)$ is
 266 a coefficient that quantifies the effect of strain on adsorption capacity. This coupling coefficient is positive
 267 for fluids that make coal swell.
 268
 269
 270
 271
 272

273 Using Equation (3), the adsorption stress can be expressed as:

$$274 S^a(P_m) = \int_0^{P_m} n_{m0}(P_m) c(P_m) V_b(P_m) dP_m \quad (4)$$

275 where V_b is the molar volume of the fluid in bulk conditions as a function of temperature and pressure. This
 276 term can be thought as an analog of thermal stress, but for adsorption (Espinoza et al., 2014). The S^a - P_m
 277 relationship for methane is shown in Figure 1a.
 278
 279
 280
 281
 282

283 The Biot coefficients (b_1 and b_3) and Biot modulus (N) are related to the coal matrix bulk modulus
 284
 285
 286
 287
 288
 289
 290
 291
 292
 293
 294
 295

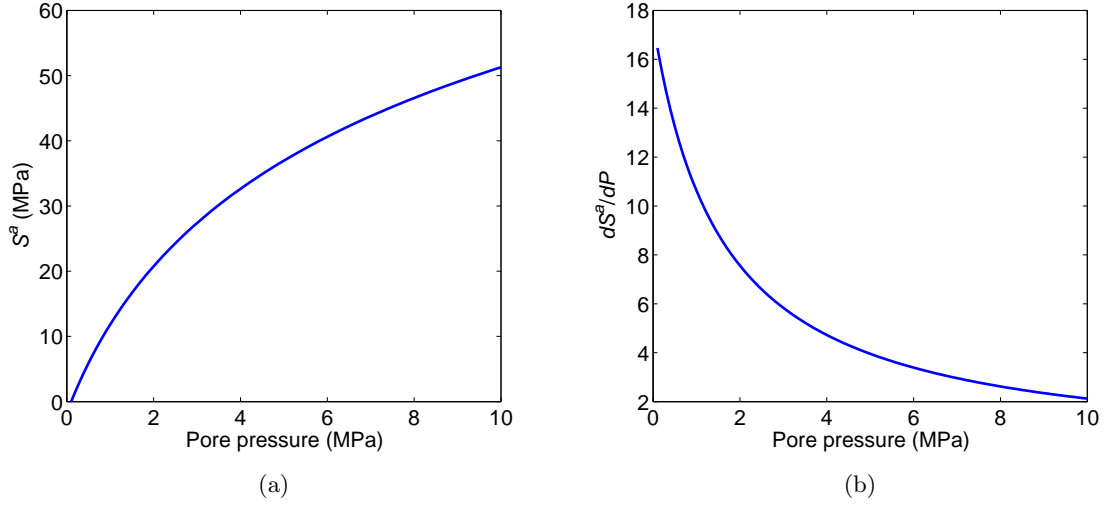


Figure 1: Adsorption stress as function of pore pressure (a) and its derivative (b).

(K_m) as follows (Coussy, 2010),

$$\begin{cases} b_1 = 1 - \frac{C_{11} + C_{12} + C_{13}}{3K_m} \\ b_3 = 1 - \frac{2C_{13} + C_{33}}{3K_m} \\ \frac{1}{N} = \frac{(2b_1 + b_3)/3 - \phi_{c0}}{3K_m} \end{cases} \quad (5)$$

According to Gibbs-Duhem equation, the pressure of fluid is related to the chemical potential as $dU = V_b(P) dP$ for isothermal conditions. In this sense, the term P_m is the pressure of the bulk fluid at the same chemical potential as the adsorbed phases in the coal matrix, termed thermodynamic pressure. In the following, the pressure of the fluid in the cleats and the thermodynamic pressure of the fluid in the coal matrix are assumed to be equal, implying fluid in the cleats is in thermodynamic equilibrium with fluid in the coal matrix at all times. Accordingly, the two terms P_c and P_m are presented by one term P , termed pore pressure. It is true that a pressure gradient can exist between the cleat and the coal matrix, especially in transient states (Peng et al., 2014). Hence, the assumption of local homogeneity of pore pressure is a limit to the applicability of the model to real cases.

The anisotropy of coal swelling (Day et al., 2008; Wang et al., 2009; Pan and Connell, 2011) is considered in the present work as a direct consequence of the anisotropy of the stiffness coefficients of the dry material. Indeed, Espinoza et al. (2013) showed that swelling anisotropy comes mostly from the anisotropy of the stiffness coefficients, and not so much from the anisotropy of the adsorption stress itself. Therefore, in the present work, we considered an isotropic adsorption stress; nevertheless, combined with anisotropic stiffness

355
356
357
358
359
360 coefficients, this isotropic adsorption stress induces an anisotropic swelling.
361

362 2.2. Permeability model

363 As mentioned previously, the permeability-change models are commonly established by two means, strain-
364 based and stress-based. We adopt here a stress-based model that correlates the logarithm of horizontal
365 permeability to the horizontal and vertical Terzaghi's effective stresses, σ , such that,
366
367
368
369

$$370 k = k_0 \exp [2\alpha_h (\Delta\sigma_h + \Delta P) + \alpha_v (\Delta\sigma_v + \Delta P)] \quad (6)$$

371
372 where k_0 is the reference horizontal permeability at a reference state. This model independently incorporates
373 the effects of the horizontal effective stress and of the vertical effective stress through introducing two cleat
374 compressibility coefficients α_h and α_v . This is different from the common used models that employed the
375 mean effective stress or the horizontal effective stress (Somerton et al., 1975; Shi and Durucan, 2004; Cui et
376 al., 2007).
377
378
379
380

381 2.3. Reference material

382 The reference coal for the analysis comes from Forzando mine in South Africa, at depth of 500 m. Several
383 cores were drilled in the horizontal and vertical directions. To calibrate the parameters of the adsorptive
384 poromechanical model and of the permeability law in Espinoza et al. (2014), experiments were performed
385 using a specifically designed triaxial cell that is able to 1) apply independently axial and radial stresses, 2)
386 measure core axial and radial deformations, 3) measure gas uptake by the coal specimen, and 4) measure core
387 permeability. The four elastic constants of dry coal specimens (E , E_3 , ν , ν_3) were measured from the stress-
388 strain data on cores (drilled horizontally and vertically) under anisotropic loading in drained conditions.
389 The coal matrix bulk modulus (K_m) was chosen as the bulk modulus of the coal core for the highest applied
390 confining stress 30 MPa. Cleat-induced Biot coefficients and Biot modulus (b_1 , b_3 , N) were then obtained
391 from Equation (5). The mean initial macroporosity (ϕ_{c0}) was estimated subtracting the microporosity of
392 coal matrix from the helium (total) porosity. The adsorptive properties (n_0^{max} , P_L , c) were obtained from
393 simultaneous fitting of 1) the coal matrix total sorption data, 2) the total uptake measured in the triaxial
394 experiments, 3) the change of strains upon injection, and 4) the measured swelling slopes upon predominant
395 adsorption regime. With regards to the permeability law, the cleat permeabilities at different horizontal
396 and vertical Terzaghi's effective stresses were measured at constant flow rate regimes. Then the values of
397 fracture compressibility parameters (α_h , α_v , k_0) were calculated.
398
399
400
401
402
403
404
405
406
407
408
409
410
411
412
413

414
415
416
417
418
419
420
421
422
423
424
425
426
427
428
429
430
431
432
433
434
435
436
437
438
439
440
441
442
443
444
445
446
447
448
449
450
451
452
453
454
455
456
457
458
459
460
461
462
463
464
465
466
467
468
469
470
471
472

Table 1: Model parameters for the reference material.

Core scale		Coal matrix		Permeability	
E	4082 MPa	K_m	5000 MPa	k_0 (10 MPa)	0.0029 mD
E_3	2551 MPa	n_0^{max}	1.2 mol/L	α_h	0.135 MPa^{-1}
ν	0.198	P_L	1.6 MPa	α_v	0.067 MPa^{-1}
ν_3	0.198	c	9		

Details of the calibration work can be found in Espinoza et al. (2014), and the best fitting parameters are summarized in Table 1. Three points should be noted. First, the adsorptive properties given in Espinoza et al. (2014) were tested with CO₂. For methane, we set $n_0^{max} = 1.2 \text{ mol/L}$ and $c = 9$, which yields an adsorption stress for methane equal to about half of the adsorption stress for CO₂ at the same pore pressure. Second, as discussed previously, the ratio E/E_3 can be greater or lower than 1 depending on the sample size. The tested coal cores in Espinoza et al. (2014) exhibited very little anisotropy. To assess the importance of the anisotropy of stiffness, we define a reference virtual fractured coal core that is more anisotropic. The vertical Young's modulus of the virtual material is identical to that of the tested coal cores $E_3 = 2551 \text{ MPa}$, but the horizontal Young's modulus is set such as $E/E_3 = 1.6$. Third, for the sake of simplification, the anisotropy of mechanical properties is assumed to totally come from the inequality between E and E_3 , so we set $\nu = \nu_3 = 0.198$.

3. Analytical models for coal permeability changes

3.1. Analytical models for different geomechanical conditions

For a representative volume element of fractured coal in oedometric condition i.e., $\Delta\varepsilon_h = 0$ and $\Delta\sigma_v = 0$, combining Equation (5) into the first three equations in Equation (1) yields:

$$\begin{aligned} \Delta\sigma_h &= \left[\frac{\nu_3 E}{(1-\nu) E_3} + \frac{E}{3K_m(1-\nu)} - 1 \right] \Delta P - \frac{E}{3K_m(1-\nu)} \Delta S^a \\ \Delta\sigma_v &= 0 \end{aligned} \tag{7}$$

We recall that the stiffness coefficients as function of Young's modulus and of Poisson ratios for transverse isotropic case are:

473
474
475
476
477
478
479
480
481
482
483
484
485
486
487
488
489
490
491
492
493
494
495
496
497
498
499
500
501
502
503
504
505
506
507
508
509
510
511
512
513
514
515
516
517
518
519
520
521
522
523
524
525
526
527
528
529
530
531

$$\begin{cases} C_{11} = \frac{E(\nu_3^2 E - E_3)}{(\nu E_3 - E_3 + 2\nu_3^2 E)(1 + \nu)} \\ C_{12} = \frac{-E(\nu_3^2 E + \nu E_3)}{(\nu E_3 - E_3 + 2\nu_3^2 E)(1 + \nu)} \\ C_{13} = \frac{-\nu_3 E E_3}{(\nu E_3 - E_3 + 2\nu_3^2 E)} \\ C_{33} = \frac{(\nu - 1) E_3^2}{(\nu E_3 - E_3 + 2\nu_3^2 E)} \end{cases} \quad (8)$$

The variation of mean Terzaghi's effective stress is:

$$\Delta \left(\frac{2\sigma_h + \sigma_v + 3P}{3} \right) = \left[\frac{2\nu_3 E}{3(1 - \nu) E_3} + \frac{2E}{9K_m(1 - \nu)} + \frac{1}{3} \right] \Delta P - \frac{2E}{9K_m(1 - \nu)} \Delta S^a \quad (9)$$

Combing Equation (7) into Equation (6), we finally obtain the pressure-permeability relationship in oedometric condition:

$$k = k_0 \exp \left(\alpha_h \left(\left[\frac{2\nu_3 E}{(1 - \nu) E_3} + \frac{2E}{3K_m(1 - \nu)} + \frac{\alpha_v}{\alpha_h} \right] \Delta P - \frac{2E}{3K_m(1 - \nu)} \Delta S^a \right) \right) \quad (10)$$

In isochoric condition, $\Delta \varepsilon_h = \Delta \varepsilon_v = 0$. Similar to the derivation in case of oedometric condition, the horizontal and vertical stresses in isochoric condition are:

$$\begin{aligned} \Delta \sigma_h &= -b_1 \Delta P - (1 - b_1) \Delta S^a \\ \Delta \sigma_v &= -b_3 \Delta P - (1 - b_3) \Delta S^a \end{aligned} \quad (11)$$

Then the pressure-dependent permeability in isochoric condition is:

$$k = k_0 \exp ([2\alpha_h (1 - b_1) + \alpha_v (1 - b_3)] (\Delta P - \Delta S^a)) \quad (12)$$

The equations of pressure-dependent permeability for different cases (Equations 10 and 12) comprise two terms: 1) variation of pressure, and 2) variation of adsorption stress. Actually, the two terms distinguish two mechanisms that govern changes in the cleat permeability. Consider reduction in pore pressure during depletion. The first term, called as a ‘‘poromechanical’’ term, leads to a cleat compression because the effective stress increases. The second term, called as an ‘‘adsorptive’’ term, causes a matrix shrinkage resulting from pressure decrease. The two terms have opposite effects: the ‘‘poromechanical’’ term results in a decrease in k , whereas the ‘‘adsorptive’’ term leads to an increase in k . The final k - P curve is the combination of the two opposing effects (Figure 2). In oedometric condition, the curve exhibits a concave shape. For

low pressure, as adsorption stress is much higher than pore pressure (Figure 1b), the “adsorptive” term predominates so the cleat permeability increases with decreasing pore pressure. However, for high pressure, dS^a/dP reduces significantly (Figure 1b) so that the “poromechanical” term becomes predominant; the cleat permeability decreases with decreasing pressure. In isochoric condition, the cleat permeability vs. pressure is a monotonic function because the adsorption stress is always greater than the pore pressure in the studied range.

In oedometric condition, it exists a rebound pressure that marks the minimum value of the cleat permeability. The rebound pressure is obtained by solving for $\partial k/\partial P = 0$, which yields:

$$\frac{dS^a}{dP} = \left[\frac{2\nu_3 E}{(1-\nu) E_3} + \frac{2E}{3K_m(1-\nu)} + \frac{\alpha_v}{\alpha_h} \right] / \left(\frac{2E}{3K_m(1-\nu)} \right) \quad (13)$$

For the reference material, Equation (13) yields $dS^a/dP = 2.9$, and the rebound pressure is 7.2 MPa. From the equation above, one can deduce that the increase of E/E_3 leads to the increase of dS^a/dP , thus the rebound pressure decreases accordingly; while the decrease of α_v/α_h results in an increase in the rebound pressure.

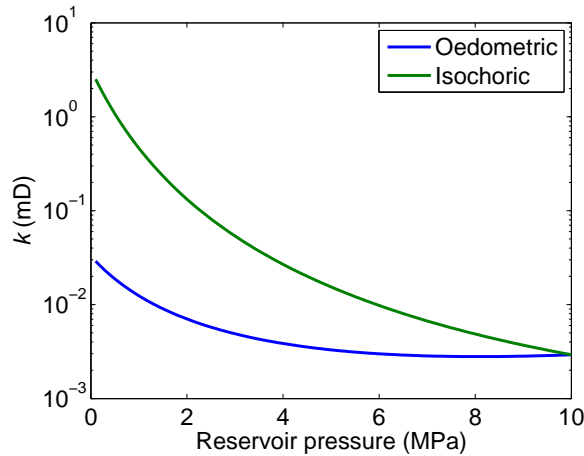


Figure 2: Evolution of permeability with reservoir pressure in oedometric and isochoric conditions at the REV scale.

3.2. Model validation

The oedometric condition is a common field condition assumed in the analytical models such as P-M model and S-D model. Broadly, our proposed model is a generalization of the relation between stresses and permeability in the S-D model: instead of only considering the dependence of permeability on the effective horizontal stress, as is the case in the S-D model, both the dependences on the horizontal and vertical

stresses are considered in our model (see Equation 10). The fact that permeability depends also on vertical (i.e., axial) stresses and not only on horizontal (i.e., radial) ones has been experimentally shown by Espinoza et al. (2014). Moreover, the adsorption property of the coal matrix is described by a term of adsorption stress in our model instead of by a term of swelling strain in S-D model.

The proposed model is verified against both field and laboratory data. Shi and Durucan (2010) used their own model to fit the San Juan basin permeability data. The same data is also matched with our model (Equation 10). Most of the model parameters (as summarized in Table 1) are not available from the field data. However, as discussed previously, the main difference of our model in comparison with the S-D model lies in Equation (6), which also considers the effect of vertical stress on the permeability change. Hence, we focus here on this difference, and the anisotropy of the poromechanical properties are neglected. The Young modulus and Poisson ratios are assumed to be identical and chosen the same as those ($E = E_3 = 2900$ MPa, $\nu = \nu_3 = 0.35$) in Shi and Durucan (2010). The model parameters regarding the coal matrix (K_m , n_0^{max} , P_L , c) for the San Juan basin coal are assumed the same as those of the reference material (Table 1). Finally, only the two cleat compressibility constants are tuned to fit the field permeability data, such that, $\alpha_h = 0.159 \text{ MPa}^{-1}$, $\alpha_v = 0.001 \text{ MPa}^{-1}$. The model match is shown in Figure 3, as well as the match using the S-D model (Shi and Durucan, 2010). Broadly, the near-exponential increase growth of absolute permeability (up to nearly 10 fold) with reservoir drawdown from 5.5 MPa is reproduced. The matched α_h value of 0.159 MPa^{-1} is greater than that (0.139 MPa^{-1}) found with the S-D model (Shi and Durucan, 2010).

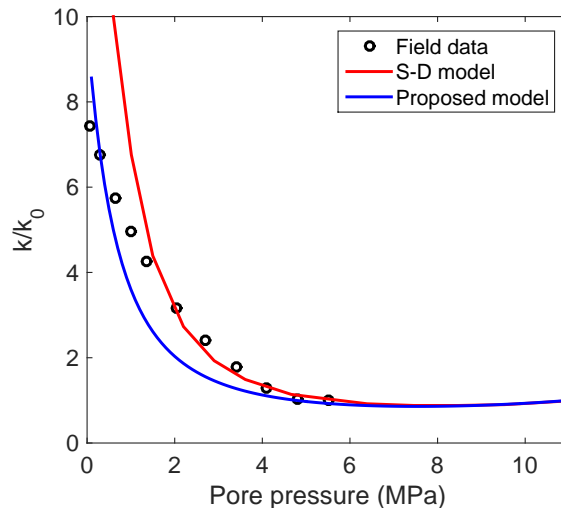


Figure 3: Model match of the San Juan basin permeability data (Shi and Durucan, 2010). The S-D model is also presented for comparison.

650
651
652
653
654
655 The performance of the proposed model (Equations 7 and 10) is also tested using the laboratory data of
656
657 Mitra et al., (2012), in which both the horizontal stress and the permeability are measured. As done in the
658
659 model match for the field data, the parameters K_m , n_0^{max} , P_L , and c are assumed the same as those of the
660
661 reference material (Table 1). The Poisson ratios (ν , ν_3) are assumed to be identical and equal to 0.3, i.e.,
662
663 the same as those in Shi and Durucan (2014), who also matched the laboratory data using their S-D model.
664
665 Since the size of the samples in Mitra et al. (2012) is comparable to the size of the samples in Espinoza et
666
667 al. (2014), we assume that $E = E_3$, as was approximately observed Espinoza et al. (2014) on their sample ¹.
668
669 Finally, only three parameters are determined by fitting the experimental data, such that, $E = 1450$ MPa,
670
671 $\alpha_h = 0.344$ MPa⁻¹, and $\alpha_v = 0.037$ MPa⁻¹. The determined values of E and α_h are both within the range
672
673 of available data (Liu et al., 2012). As shown in Figure 4, the proposed model can reproduce appropriately
674
675 both the horizontal stress and the permeability. The deviation of the predicted horizontal stress for the
676
677 lowest two pressure points (when P is less than 1.4 MPa) can be explained by the reduction in Young’s
678
679 modulus at low pore pressure (Shi et al., 2014; Shi and Durucan, 2018).

675
676 The same experimental data has also been matched by Shi et al. (2014) using their own model. Applying a
677
678 constant α_h value of 0.194 MPa⁻¹, the S-D model well reproduced the laboratory results when pore pressure
679
680 varied from 6.2 MPa to 1.4 MPa but failed to match the data when the pore pressure reduced below 1.4
681
682 MPa (Figure 4). In contrast, the proposed model succeeds in fitting the whole experimental data using a
683
684 constant α_h value.

684 4. The role of anisotropy

686 4.1. Analytical modeling at the scale of representative volume element

688 4.1.1. The role of the anisotropy of stiffness

689
690 In the following, the role of different anisotropy terms on the k - P relationship will be explored. To do so,
691
692 three types of equivalent materials are established: the first neglecting the anisotropy of stiffness, the second
693
694 neglecting the anisotropy of permeability dependence on stresses, and the third neglecting both anisotropies.
695
696 The coefficients of these equivalent materials are calibrated on the permeability variations predicted with
697
698 the anisotropic model (Figure 2). Comparisons are conducted to assess how well the equivalent isotropic
699
700 models can reproduce the permeability variations predicted with the anisotropic model, and thus the role
701
702 of the different types of anisotropy can be discussed.

701
702 ¹the anisotropy of the elastic properties is indeed expected to be somehow related to the size of the sample, since, in
703
704 particular because of the presence of cleats, elastic properties are known to depend on the size of the sample

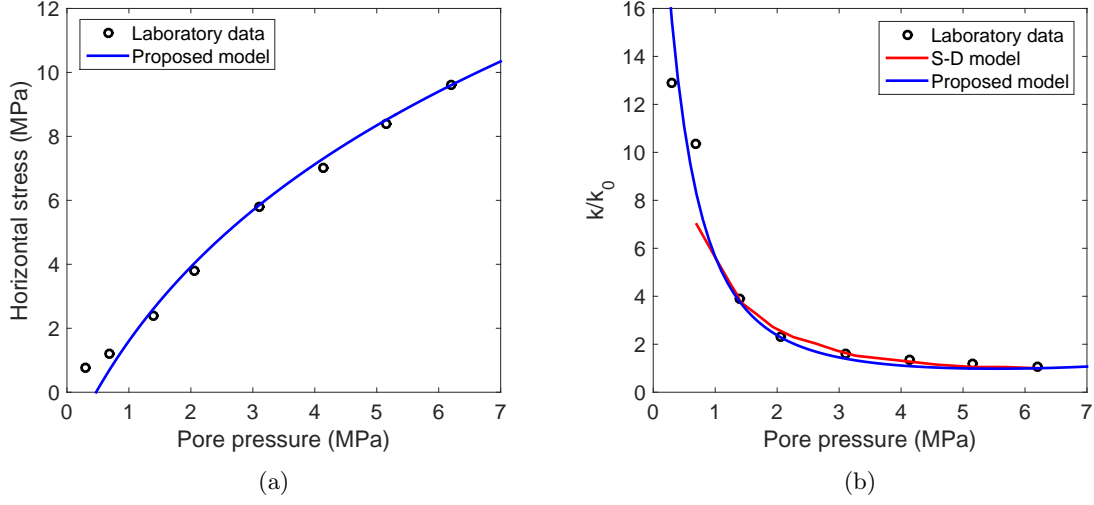


Figure 4: Validation of the proposed model using laboratory data of (Mitra et al., 2012): a) horizontal stress, b) permeability. The S-D model (Shi et al., 2014) is also presented for comparison.

As mentioned previously, the anisotropy of stiffness in the present work specifically refers to the difference between E and E_3 . To evaluate its importance for the k - P relationship, we consider an equivalent isotropic material. The two elastic constants are assessed in two ways. In the first way (called free K method), the Young's modulus and Poisson ratio of the equivalent isotropic material are calculated such that its volumetric Terzaghi's effective stress in oedometric condition (refer to Equation 9) is identical to that of anisotropic material:

$$\begin{aligned} \frac{\nu^{ia}}{1 - \nu^{ia}} &= \frac{\nu_3 E}{(1 - \nu) E_3} \\ \frac{E^{ia}}{(1 - \nu^{ia})} &= \frac{E}{(1 - \nu)} \end{aligned} \quad (14)$$

We obtain $E^{ia} = 3648$ MPa and $\nu^{ia} = 0.283$. The superscript ia stands for the equivalent material with isotropic stiffness and anisotropic permeability dependence on stresses. For this isotropic material, still employing the same anisotropic permeability dependence on stresses as for the reference anisotropic material, we predict exactly the same k - P curve with respect to the reference anisotropic material in oedometric condition, shown in Figure 5a. Actually, in oedometric condition, the equivalence of the volumetric Terzaghi's effective stress (i.e., $2\sigma_h/3 + P$) implies the equivalence of the horizontal stress. Hence, the anisotropy of stiffness can be neglected without introducing any error. However, using the free K method, the bulk modulus of the isotropic material ($1/K^{ia} = 3(1 - \nu)/E - 3\nu_3/E_3$) is skewed (the isotropic bulk modulus of the anisotropic materials is $1/K = 2(1 - \nu)/E + (1 - 4\nu_3)/E_3$), shown in Figure 6. To avoid the mismatch

768
769
770
771
772
773 in bulk modulus, we propose another method (called constrained K method): the bulk modulus K is
774 constrained, and the second elastic constant (ν^{ia}) is obtained by fitting the pressure-permeability curve in
775 oedometric condition, i.e., minimizing $(\log k_{iso}^s - \log k)^2$. The fitting yields $\nu^{ia} = 0.219$. This constrained
776 K method can result in an almost perfect reproduction of the P - k curve with respect to the reference
777 anisotropic material (see Figure 5a).
778
779

780
781 To quantify the error induced by disregarding different terms of anisotropy, we define an error norm i.e., e
782 $= \text{mean}(|\log(k_{iso}^i/k)|)$, where i might refer to s (in case of disregarding the anisotropy of stiffness), p (in case
783 of disregarding the anisotropy of permeability dependence on stresses) or sp (in case of disregarding both
784 anisotropies of stiffness and of permeability dependence on stresses). We carry out a parametric analysis
785 varying α_h and E with constrained α_v and E_3 , and the results in case of disregarding the anisotropy of
786 stiffness are shown in Figure 7, for both oedometric and isochoric conditions. In general, both methods
787 reproduce well the pressure-permeability curve in oedometric condition, for which the averaged k_{iso}^s/k is
788 less than $10^{0.05} = 1.1$. Using the constrained K method, the error increases with the anisotropy degree of
789 stiffness and of permeability dependence on stresses.
790
791

792
793 The elastic constants of equivalent isotropic material calibrated in oedometric condition are applied
794 for the prediction of the P - k curve in isochoric condition, shown in Figure 5b. In general, the free K
795 method overestimates the cleat permeability, whereas the constrained K method underestimates the cleat
796 permeability. This trend can be explained by Equation 12, considering b^{ia} equal to 0.44 and 0.58 for the free
797 and constrained K methods, respectively (compared to $b_1 = 0.52$ and $b_3 = 0.64$). Regarding the absolute
798 value of the errors, the constrained K method provides better prediction in isochoric condition: the average
799 of k_{iso}^s/k is $10^{0.25} = 1.8$ using the constrained K method; whereas, it can reach $10^{0.60} = 4.0$ using the free
800 K method (Figure 7c and 7d).
801
802
803
804
805
806
807

808 4.1.2. The role of the anisotropy of permeability dependence on stresses

809
810 We now evaluate the importance of the anisotropy of permeability dependence on stresses. To do so,
811 while keeping the anisotropic elastic properties unchanged, we consider a permeability that only depends
812 on the volumetric stress so that the two coefficients α_h and α_v are replaced by a single coefficient α^{ai} .
813 This coefficient is determined by fitting the P - k curve using the same principle as for the identification of
814 the second elastic constant of the equivalent isotropic material using constrained K method: it yields α^{ai}
815 $= 0.156 \text{ MPa}^{-1}$. For this virtual material that obeys isotropic permeability dependence on stresses, the
816 pressure-permeability curve is below that for the reference material in oedometric condition (Figure 5c);
817 whereas, the permeability is overestimated in isochoric condition (Figure 5d). The fitted value α^{ai} depends
818
819
820
821
822
823
824
825
826

on α_h/α_v as well as E/E_3 : it may be beyond the $[\alpha_v, \alpha_h]$ interval; it can be even negative in some cases (Figure 8).

The error e on permeability induced when disregarding the anisotropy of permeability dependence on stresses is shown in Figure 9. It is normal to observe that the error increases with α_h/α_v . The dependence of the error with E/E_3 is more complex. In oedometric condition, the error increases with E/E_3 up to a maximum and then reduces slightly (Figure 9b). In isochoric condition, two troughs exist in the e - E/E_3 curve: the first is at lowest E/E_3 value, while the second is close to 1.4 with $e = 0$ regardless of the α_h/α_v value (Figure 9d).

Compared to neglecting the anisotropy of stiffness, disregarding the anisotropy of permeability leads to larger deviations from the k - P curves in the anisotropic case: in the tested α_h/α_v and E/E_3 intervals, the averaged k_{iso}^p/k in oedometric and isochoric conditions can reach nearly $10^{0.3} = 2.0$ and $10^{1.2} = 15.8$, respectively, in comparison to $10^{0.05} = 1.1$ and $10^{0.25} = 1.8$ when neglecting the anisotropy of stiffness.

4.1.3. Disregarding both anisotropies of stiffness and of permeability dependence on stresses

We now consider the case where both anisotropies of stiffness and of permeability dependence on stresses are neglected. In this totally isotropic case, the material properties reduce to three: one for the permeability law (α^{ii}) and two for the stiffness (E^{ii} and ν^{ii}). To assess the three parameters, a method comparable to that used for investigating the role of the anisotropy of stiffness is applied again: the two coefficients before the pore pressure and adsorption stress terms are identical in anisotropic and totally isotropic cases for oedometric condition (Equation 10). Since the oedometric condition only leads to two equations for three unknowns, the system is underdetermined. The third equation can be introduced by equating the P - k curves in isochoric condition (Equation 12). Thus,

$$\begin{aligned} \frac{2\nu_3 E \alpha_r}{(1-\nu) E_3} + \frac{2E \alpha_r}{3K_m (1-\nu)} + \alpha_a &= \frac{2\nu^{ii} \alpha^{ii}}{1-\nu^{ii}} + \frac{2E^{ii} \alpha^{ii}}{3K_m (1-\nu^{ii})} + \alpha^{ii} \\ \frac{2E \alpha_r}{3K_m (1-\nu)} &= \frac{2E^{ii} \alpha^{ii}}{3K_m (1-\nu^{ii})} \\ 2\alpha_r (1-b_1) + \alpha_a (1-b_3) &= 3\alpha^{ii} (1-b^{ii}) \end{aligned} \quad (15)$$

For the totally isotropic material, Equation (15) yields $E^{ii} = 4342$ MPa, $\nu^{ii} = 0.099$, and $\alpha_{ii} = 0.142$ MPa⁻¹. This leads to an exact reproduction of the k - P curves in both oedometric and isochoric conditions (Figures 5e and 5f). However, as for the case of disregarding the anisotropy of stiffness, the bulk modulus of the totally isotropic material is skewed respect to the bulk modulus of the reference anisotropic material (Figure 10). Moreover, this equivalent totally isotropic material cannot reproduce the same P - k curves in

886
887
888
889
890
891 other geomechanical conditions, and the error might be more significant than for the case when only one
892 term of anisotropy is neglected. We provide here two examples: free swelling condition (i.e., $\Delta\sigma_r = \Delta\sigma_a =$
893 0) and inverse oedometric condition (i.e., $\Delta\sigma_r = 0, \Delta\varepsilon_a = 0$), shown in Figure 11.
894
895

896 897 *4.2. Numerical simulation at the scale of reservoir*

898
899 In the section above, the role of anisotropy in permeability changes was investigated at the scale of
900 representative element volume, and some geomechanical assumptions were employed in the derivation of the
901 analytical equations, e.g., the assumption of uniaxial strain and constant vertical stress (i.e. of oedometric
902 condition). These assumptions do not exactly match the coalbed conditions for real methane recovery at the
903 scale of reservoir, and so the accuracy of the analytical modeling should be investigated. For instance, oedo-
904 metric condition is the most common condition used for matching CBM production (Palmer and Mansoori,
905 1998; Shi and Durucan, 2004). During the production, subsidence and pressure gradients lead to creation
906 of shear stress as well as changes in vertical stress (Settari, 2002). Moreover, there is field evidence that the
907 uniaxial strain assumption may not be accurate during reservoir subsidence (Connell, 2009).
908
909

910
911 This section is devoted to assessing how formation permeability changes with declining reservoir pres-
912 sure. Once the pressure-permeability relationship is established independently, the analytical models and
913 subsequent analysis obtained in the previous section can be tested in how well they match the response at
914 the reservoir scale. To do so, reservoir simulations are performed considering the same four materials as
915 in the previous section. 1) A totally anisotropic reference material with material properties given in Table
916 1. 2) An equivalent isotropic material, but the permeability of which still depends in different manners on
917 horizontal and vertical effective stresses. The isotropic mechanical constants are $E^{ia} = 3648$ MPa and $\nu^{ia} =$
918 0.283 . 3) An anisotropic material, but with the permeability that only depends on the volumetric stress: its
919 cleat compressibility is $\alpha_{ai} = 0.156$ MPa⁻¹. 4) A fully isotropic material: its elastic properties are isotropic
920 ($E^{ii} = 4342$ MPa and $\nu^{ii} = 0.099$), and its permeability only depends on the volumetric stress ($\alpha^{ii} = 0.142$
921 MPa⁻¹).
922
923
924
925
926
927
928

929
930 We model the depletion of a coal seam containing pure methane at 312.15 K. Vertical and horizontal in-
931 situ total stresses are 23 MPa and 14 MPa, respectively; initial pressure of methane is 10 MPa. Simulation is
932 axisymmetrical. The radius of the borehole is 0.1 m. The radius of the coal seam is 100 m, its thickness is 5
933 m. 30-m-thick impervious isotropic cap rock and bed rock are considered in the simulation, their mechanical
934 properties are: $E_c = 10$ GPa and $\nu_c = 0.26$. The simulation is conducted through the in-house software
935 “Bil” based on the finite element method. The mesh (with a total element number of 21571) used in the
936 simulations is displayed in Figure 12, together with the mechanical boundary conditions. With regards to
937
938
939

945 the hydraulic boundary conditions in the coal seam, flow is null at outer boundary. Two types of boundary
946 conditions are considered at the borehole: constant production rate (0.001 mol/(s.m²)) and constant pressure
947 (1 MPa). In case of constant production rate, the small rate is employed so that methane can be recovered
948 more fully and the reservoir pressure can fall to a low value (down to 5MPa in our simulation) to maintain
949 this production rate. This enables obtaining the permeability variation curve in a wide pressure range. We
950 consider that the kinetics of methane flowing from the coal matrix to the cleats is very fast: at any time, at
951 any location in the coal seam, the pressure of the fluid in the cleats and the thermodynamic pressure of the
952 fluid in the coal matrix are considered to be equal.

963 4.2.1. Estimation of reservoir permeability

964 The reservoir simulation gives rise to production data including gas rate history, evolution of pressure
965 profile in the reservoir. These data are then used to calculate the formation permeability k_g (in mD) using
966 the production data analysis method (Lee et al., 1984; Clarkson, 2007):
967

$$970 k_g = \frac{q_g T [\ln(r_e/r_w) - 0.5 + s + Dq_g]}{7.03 \times 10^{-4} h [m(P_r) - m(P_{wf})]} \quad (16)$$

971 where r_e and r_w are drainage radius and wellbore radius, q_g is gas surface flow rate, m is pseudo-pressure (in
972 psi²/cp), P_r and P_{wf} stand for reservoir pressure and bottomhole pressure, s is skin factor (assumed equal
973 to 0 here), and D is inertial or turbulent flow factor (in D/Mscf, assumed equal to 0 here). In the following,
974 the reservoir pressure P_r is equal to the pressure at the outer boundary P_e . The derivation of Equation
975 (16) is based on the pseudo-steady-state analytical solution of a radial flow from a finite cylindrical reservoir
976 at a constant production rate, and the derivation details are provided in Appendix A. It should be noted
977 that our equation slightly differs from the equation in the literature (Lee et al., 1984; Clarkson, 2007): the
978 constant 0.75 is modified into 0.5.
979

980 To validate Equation (16), we model recovery of methane from a coal seam with invariant permeability
981 (i.e., $\alpha_h = \alpha_v = 0$). The other mechanical and permeability properties are the same as the reference
982 material. Equation (16) is valid for the pseudo-steady-state, i.e., $t_D > 0.3r_e^2$ (refer to Appendix A). For the
983 considered system, the time for reaching the pseudo-steady-state is 4.5 years. After this time, the estimated
984 reservoir permeability agrees well with the coal permeability, which validates Equation (16).
985

994 4.2.2. Reservoir simulation results

995 The profiles of pore pressure at different times in two cases (i.e., constant flow and constant pressure)
996 are shown in Figure 13; the evolution of borehole pressure and pressure at outer boundary is displayed in
997

1004
1005
1006
1007
1008
1009
1010
1011
1012
1013
1014
1015
1016
1017
1018
1019
1020
1021
1022
1023
1024
1025
1026
1027
1028
1029
1030
1031
1032
1033
1034
1035
1036
1037
1038
1039
1040
1041
1042
1043
1044
1045
1046
1047
1048
1049
1050
1051
1052
1053
1054
1055
1056
1057
1058
1059
1060
1061
1062

Figure 14. Given the range of applicability of Equation (16), the pressure-permeability curve is estimated only after 4.5 years or more have elapsed since methane production started. The k - P curve determined from the reservoir simulation is shown in Figure 15. The analytical model curves for oedometric and isochoric conditions also are given for comparison. One observes that oedometric condition gives a good representation of the reservoir. Compared to the constant-pressure condition, the constant-flow condition gives rise to a k - P curve more consistent with that for the analytical oedometric condition. This is mainly because Equation (16) is derived from the analytical solution of the flow equation in case of constant production rate.

When the anisotropic material is simplified by an equivalent material with isotropic stiffness using Equation (14), we reproduce the same k_g - P curve as in the reference anisotropic case. This is also the case when both anisotropies of stiffness and of permeability dependence on stresses are disregarded. When neglecting the anisotropy of permeability dependence on stresses, the pressure-dependent permeability curve deviates from the curve for the anisotropic material: for the reference material considered, it underestimates the reservoir permeability. These observations at the scale of reservoir are comparable with those obtained from analytical modeling at the scale of representative element volume.

5. Conclusion

The effect of anisotropy on the horizontal permeability changes in coal seams was investigated. The analysis was based on a fully anisotropic model consisting of both the anisotropies of stiffness and of how horizontal permeability depends on stress. The main findings include:

- The analytical expression of the horizontal permeability changes in oedometric condition is derived. Different from the existing models that merely considered the dependence of the horizontal permeability on the horizontal stress or on the mean stress, the proposed model separately incorporates the effects of the horizontal effective stress and of the vertical effective stress. Moreover, the mechanical anisotropy is also taken into account. The proposed model is validated against both available laboratory and field data.
- On the basis of the analytical expression, we demonstrate that the mechanically anisotropic materials can be simplified by an isotropic material without introducing any error in permeability changes (called free K method). However, this free K method leads to a fitted bulk modulus that differs from the actual bulk modulus of the material, and results in significant errors on the permeability variations estimated in isochoric condition. Hence, an alternative method with constrained K (i.e., with a bulk

modulus that is kept equal to the actual bulk modulus of the material) is proposed: it still provides a very good estimate of permeability changes in oedometric condition, while providing an estimate of permeability variations in isochoric condition which is better than with the free K method.

- The anisotropy of permeability dependence on stresses plays a predominant role in the permeability changes in coal seams. Indeed, over the range of parameters here considered, when disregarding the anisotropy of cleat compressibility (α), the permeability can be misestimated by a ratio of up to 15.8. In comparison, when disregarding the anisotropy of stiffness, the permeability can be misestimated by a maximal ratio of only 1.8.
- The errors on the estimated permeability by disregarding the two terms of anisotropies depend on α_h/α_v and E/E_3 . In general, the increase in the anisotropy degree of permeability dependence on stresses translates into an increase of the error. Nevertheless, the effect of mechanical anisotropy on the error is more complex and not monotonic. In some cases (typically when $E/E_3 < 1$), the error induced by disregarding the anisotropy of permeability dependence on stresses can decrease with an increasing mechanical anisotropy.
- When both anisotropies of stiffness and of permeability dependence on stresses are neglected, the material constants can be assessed in such a way that the k - P curve can be exactly reproduced in both oedometric and isotropic conditions. However, in such case, the fitted bulk modulus is not equal to the bulk modulus of the actual material. Moreover, the totally isotropic material cannot reproduce the variation of permeability in conditions other than oedometric or isochoric.
- The pressure-dependent permeability curve also is determined at the reservoir scale. The reservoir simulation results confirm the conclusions obtained from the analytical modeling at the scale of a representative elementary volume.

Appendix A. Estimation of permeability-pressure relationship from production data

Consider a radial flow from a finite cylindrical reservoir (with sealed upper and lower surfaces) at a constant production rate. The flow at the outer boundary is zero at all times. The flow equation for a cylindrical flow described in terms of dimensionless variables is (Board, 1979):

$$\frac{1}{r_D} \frac{\partial}{\partial r_D} \left[r_D \frac{\partial}{\partial r_D} (\Delta P_D) \right] = \frac{\partial}{\partial t_D} (\Delta P_D) \quad (\text{A.1})$$

The boundary and initial conditions are: a) The flow rate at the well is constant,

$$r_D \frac{\partial}{\partial r_D} (\Delta P_D) \Big|_{r_D=1} = -1 \quad (\text{A.2})$$

b) The flow at the outer boundary is zero,

$$\frac{\partial}{\partial r_D} (\Delta P_D) \Big|_{r_{eD}} = 0 \quad (\text{A.3})$$

c) The initial reservoir pressure is uniform,

$$\Delta P_D = 0 \quad (\text{A.4})$$

The dimensionless variables are defined as:

$$r_D = \frac{r}{r_w} \quad (\text{A.5})$$

$$t_D = \frac{\lambda k t}{\phi \mu_i c_i^f r_w^2} \quad (\text{A.6})$$

$$\Delta P_D = \frac{m_i - m}{m_i q_D} \quad (\text{A.7})$$

$$q_D = \frac{\gamma T q_{st}}{k h m_i} \quad (\text{A.8})$$

where k is permeability, ϕ is porosity, μ is viscosity of fluid, c^f is compressibility of fluid, h is the formation thickness. The subscript i stands for the initial condition. The two coefficient λ and γ include coefficient like 2 and π , units conversion factors, and the numerical values of P_{st} and T_{st} that may be inherent in the definitions of the dimensionless terms. The pseudo-pressure m is defined as:

$$m = 2 \int_{P_0}^P \frac{P}{\mu Z} dP \quad (\text{A.9})$$

where P_0 is a specified reference pressure. The compressibility factor, Z , is a correlation factor which defines the deviation of a real gas from ideal gas behaviour.

If the well radius can be assumed to be vanishingly small (i.e., $r_e \gg r_w$), the general solution of the problem is:

$$\Delta P_D(t_D) = \frac{2}{r_{eD}^2} \left(\frac{r_D^2}{4} + t_D - \frac{r_{eD}^2 \ln r_D}{2} \right) - \frac{3}{4} + \ln r_{eD} + \sum_{n=1}^{\infty} \frac{\pi J_1^2(\alpha_n r_{eD}) U_n(\alpha_n r_D)}{\alpha_n [J_1^2(\alpha_n r_{eD}) - J_1^2(\alpha_n)]} e^{-\alpha_n^2 t_D} \quad (\text{A.10})$$

where α_n are the roots of

$$J_1(\alpha_n r_{eD}) Y_1(\alpha_n) - J_1(\alpha_n) Y_1(\alpha_n r_{eD}) = 0 \quad (\text{A.11})$$

J_1 and Y_1 are Bessel functions of the first and second kind, respectively and both of order one.

When t_D is sufficient large ($t_D > 0.3r_{eD}^2$), the summation term in Equation A.10) becomes negligible, and the pressure at the well and at the outer boundary are simply:

$$\Delta P_D|_{r_D=1} = \frac{2t_D}{r_{eD}^2} - 0.75 + \ln r_{eD} \quad (\text{A.12})$$

$$\Delta P_D|_{r_{eD}} = \frac{2t_D}{r_{eD}^2} - 0.25 \quad (\text{A.13})$$

Combining the two above equations and using the definition of the dimensionless variables, we obtain,

$$m(P_r) - m(P_{wf}) = \frac{\gamma T q_{st}}{kh} (\ln r_{eD} - 0.5) \quad (\text{A.14})$$

In the derivation above, it was assumed that the medium is homogeneous and isotropic and that flow is single-phase and obeys Darcy's law. In real case, deviations from these idealizations are frequent and can not be ignored. Two terms commonly are considered: 1) the skin effect to account for the altered permeability at the vicinity of well because of well drilling, fracturing or acidizing on completion; 2) the inertial /turbulent flow effect that are not taken into account by Darcy's law. Taking the two effects into account, we finally obtain the equation for estimating the formation permeability by production data.

References

- Board, E.R.C., 1979. Gas Well Testing: Theory and Practice. Energy Resources Conservation Board.
- Brochard, L., Vandamme, M., Pellenq, R.J.M., 2012. Poromechanics of microporous media. Journal of Mechanics and Physics of Solids 60, 606-622.
- Cheng, A.D., 1997. Material coefficients of anisotropic poroelasticity. International Journal of Rock Mechanics and Mining Science 34, 199-205.
- Clarkson, C.R., Jordan, C.L., Gierhart, R.R., Seidle, J.P., 2007. Production data analysis of CBM wells. SPE107705.
- Coussy, O., 2010. Mechanics and Physics of Porous Solids. Wiley.

- 1240
1241
1242
1243
1244
1245 Cui, X., Bustin, R.M., 2005. Volumetric strain associated with methane desorption and its impact on coalbed gas production
1246 from deep coal seams. *American Association of Petroleum Geologists Bulletin* 89 (9), 1181-1202.
1247
1248 Cui, X., Bustin, R.M., Chikatamarla, L., 2007. Adsorption-induced coal swelling and stress: implications for methane production
1249 and acid gas sequestration into coal seams. *Journal of Geophysical Research* 112, B10202.
1250
1251 Connell, L.D., 2009. Coupled flow and geomechanical processes during gas production from coal seams. *International Journal*
1252 *of Coal Geology* 79, 18-28.
1253
1254 Day, S., Fry, R., Sakurovs, R., 2008. Swelling of Australian coals in supercritical CO₂. *International Journal of Coal Geology*
1255 74, 41-52.
1256
1257 Espinoza, D.N., Vandamme, M., Dangla, P., Pereira, J.M., Vidal-Gilbert, S., 2013. A transverse isotropic model for microporous
1258 solids: Application to coal matrix adsorption and swelling. *Journal of Geophysical Research: Solid Earth* 118(12), 6113-6123.
1259
1260 Espinoza, D.N., Vandamme, M., Pereira, J.M., Dangla, P., Vidal-Gilbert, S., 2014. Measurement and modeling of adsorptive-
1261 poromechanical properties of bituminous coal cores exposed to CO₂: adsorption, swelling strains, swelling stresses and
1262 impact on fracture permeability. *International Journal of Coal Geology* 134-135, 80-95.
1263
1264 Hol, S., Spiers, C.J., 2012. Competition between adsorption-induced swelling and elastic compression of coal at CO₂ pressures
1265 up to 100MPa. *Journal of the Mechanics and Physics of Solids* 60, 1862-1882.
1266
1267 Laubach, S.E., Marrett, R.A., Olson, J.E., Scott, A.R., 1998. Characteristics and origins of coal cleat: a review. *International*
1268 *Journal of Coal Geology* 35, 175-207.
1269
1270 Lee, W.J., Kuo, T.B., Holditch, S.A., McVay, D.A., 1984. Estimating formation permeability from single-point flow data,
1271 SPE/DOE/GRI12847.
1272
1273 Liu, S., Harpalani, S., Mitra, A., 2012. Laboratory measurement and modelling of coal permeability with continued methane
1274 production: part 2 - Modelling results. *Fuel* 94, 117-124.
1275
1276 Mitra, A., Harpalani, S., Liu, S.M., 2012. Laboratory measurement and modeling of coal permeability with continued methane
1277 production: Part 1 - Laboratory results. *Fuel* 94, 110-116.
1278
1279 Morcote, A., Mavko, G., Prasad, M., 2010. Dynamic elastic properties of coal. *Geophysics* 75, E227-E234.
1280
1281 Nikoosokhan, S., Vandamme, M., Dangla, P., 2014. A poromechanical model for coal seams saturated with binary mixtures of
1282 CH₄ and CO₂. *Journal of the Mechanics and Physics of Solids* 71, 97-111.
1283
1284 Palmer, I., 2009. Permeability changes in coal: analytical modeling. *International Journal of Coal Geology* 77, 119-126.
1285
1286 Palmer, I., Mansoori, J., 1998. How permeability depends on stress and pore pressure in coalbeds: a new model. *SPE Reservoir*
1287 *Evaluation & Engineering*, 539-544.
1288
1289 Palmer, I.D., Mavor, M., Gunter, B., 2007. Permeability changes in coal seams during production and injection. *International*
1290 *Coalbed Methane Symposium*. University of Alabama, Tuscaloosa, Alabama. Paper 0713.
1291
1292 Pan, Z.J., Connell, L.D., 2007. A theoretical model for gas adsorption-induced coal swelling. *International Journal of Coal*
1293 *Geology* 69, 243-252.
1294
1295 Pan, Z.J., Connell, L.D., 2011. Modelling of anisotropic coal swelling and its impact on permeability behaviour for primary
1296 and enhanced coalbed methane recovery. *International Journal of Coal Geology* 85, 257-267.
1297
1298 Peng, Y., Liu, J., Wei, M., Pan, Z., Connell, L.D., 2014. Why coal permeability changes under free swellings: New insights.
1299 *International Journal of Coal Geology*, 133, 35-46.
1300
1301 Pone, J.D.N., Halleck, P.M., Mathews, J.P., 2010. 3D characterization of coal strains induced by compression, carbon dioxide
1302 sorption, and desorption at in-situ stress conditions. *International Journal of Coal Geology* 82, 262-268.

- 1299
1300
1301
1302
1303
1304 Seidle, J.P., Jeansonne, M.W., Erickson, D.J., 1992. Application of matchstick geometry to stress dependent permeability in
1305 coals. Rocky Mountain Regional Meeting of the Society of Petroleum Engineers. Casper, Wyoming. SPE 24361.
1306
1307 Settari, A., 2002. Reservoir compaction. *Journal of Petroleum Technology* 54(8), 62-69.
1308 Shi, J.Q., Durucan, S., 2004. Drawdown induced changes in permeability of coalbeds: a new interpretation of the reservoir
1309 response to primary recovery. *Transport in Porous Media* 56(1), 1-16.
1310 Shi, J.Q., Durucan, S., 2010. Exponential growth in San Juan basin Fruitland coalbed permeability with reservoir drawdown:
1311 model match and new insights. *SPE Reservoir Evaluation & Engineering* 13(6), 914-925.
1312 Shi, J.Q., Durucan, S., 2014. Modelling laboratory horizontal stress and coal permeability data using S&D permeability model.
1313 *International Journal of Coal Geology* 131, 172-176.
1314 Shi, J.Q., Pan, Z., Durucan, S., 2014. Analytical models for coal permeability changes during coalbed methane recovery: Model
1315 comparison and performance evaluation, *International Journal of Coal Geology* 136, 17-24.
1316 Shi, J.Q., Durucan, S., 2018. Variation in horizontal stress with pore pressure depletion in coal under uniaxial strain conditions:
1317 An update on the modelling of laboratory data, *International Journal of Coal Geology* 187, 94-97.
1318 Somerton, W.H., Soylemezolu, I.M., Dudley, R.C., 1975. Effect of stress on permeability of coal. *Journal of Rock Mechanics*
1319 *and Mining Science & Geomechanics Abstracts* 12, 129-145.
1320 Vandamme, M., Brochard, L., Lecampion, B., Coussy, O., 2010. Adsorption and strain: the CO₂-induced swelling of coal.
1321 *Journal of Mechanics and Physics of Solids* 58, 1489-1505.
1322 Wang, G.X., Massarotto, P., Rudolph, V., 2009. An improved permeability model of coal for coalbed methane recovery and
1323 CO₂ geosequestration. *International Journal of Coal Geology* 77, 127-136.
1324 Wang, J.G., Liu, J.S., Kabirc, A., 2013. Combined effects of directional compaction, non-Darcy flow and anisotropic swelling
1325 on coal seam gas extraction. *International Journal of Coal Geology* 109-111, 1-14.
1326 Wang, K., Zang, J., Wang, G.D., Zhou, A.T., 2014. Anisotropic permeability evolution of coal with effective stress variation
1327 and gas sorption: Model development and analysis. *International Journal of Coal Geology* 130, 53-65.
1328
1329
1330
1331
1332
1333
1334
1335
1336
1337
1338
1339
1340
1341
1342
1343
1344
1345
1346
1347
1348
1349
1350
1351
1352
1353
1354
1355
1356
1357

1358
1359
1360
1361
1362
1363 Glossary
1364

1365 b_1, b_3 : Horizontal and vertical Biot coefficient [-]

1366 c : Adsorption-strain coupling coefficient [-]
1367

1368 C_{ij} : Stiffness tensor coefficient defined at the coal seam scale [Pa]

1369 D : Inertial or turbulent flow factor [D/Mscf]
1370

1371 E, E_3 : Horizontal and vertical Young's modulus [Pa]
1372

1373 h : Formation thickness [ft]

1374 k : Coal horizontal permeability [mD]

1375 k_0 : Reference coal horizontal permeability (at 10 MPa) [mD]
1376

1377 k_g : Reservoir horizontal permeability [mD]
1378

1379 K : Coal seam bulk modulus [Pa]

1380 K_m : Coal matrix bulk modulus [Pa]
1381

1382 $m(P)$: Pseudopressure [psi^2/cp]

1383 n_m : Fluid amount in the coal matrix per unit volume of coal matrix [mol/L]
1384

1385 n_0^{max} : Asymptotic parameter of constant matrix volume Langmuir isotherm [mol/L]
1386

1387 n_T : Total fluid amount per unit volume of coal seam REV [mol/L]

1388 N : Coal seam Biot modulus [Pa]
1389

1390 P : Pore pressure ($P = P_c = P_m$) [Pa]

1391 P_c : Pressure of fluid in the cleat [Pa]
1392

1393 P_e : Pressure at the outer boundary in the simulation [Pa]

1394 P_L : Langmuir pressure of constant matrix volume Langmuir isotherm [Pa]
1395

1396 P_m : Thermodynamical pressure of fluid in the coal matrix [Pa]

1397 P_r : Reservoir pressure [psia]
1398

1399 P_{wf} : Flowing bottomhole pressure [psia]

1400 q_g : Gas surface flow rate [Mscf/D]
1401

1402 r_e : Drainage radius [ft]

1403 r_w : Wellbore radius [ft]
1404

1405 s : Skin factor [-]

1406 S^a : Coal matrix adsorption stress [Pa]
1407

1408 T : Temperature [$^{\circ}\text{R}$]
1409

1410 U : Chemical potential [J/mol]
1411

1417
1418
1419
1420
1421
1422
1423
1424
1425
1426
1427
1428
1429
1430
1431
1432
1433
1434
1435
1436
1437
1438
1439
1440
1441
1442
1443
1444
1445
1446
1447
1448
1449
1450
1451
1452
1453
1454
1455
1456
1457
1458
1459
1460
1461
1462
1463
1464
1465
1466
1467
1468
1469
1470
1471
1472
1473
1474
1475

V_b : Molar volume of the fluid in bulk conditions [L/mol]

Subscript

1,2: Horizontal

3: Vertical

D : Dimensionless

h : Horizontal direction

v : Vertical direction

Superscript

ia : In case of isotropic stiffness and anisotropic permeability dependence on stresses

ai : In case of anisotropic stiffness and isotropic permeability dependence on stresses

ii : In case of isotropic stiffness and isotropic permeability dependence on stresses

Greek symbols

α : Cleat compressibility coefficient for permeability law [MPa⁻¹]

ε_m : Volumetric strain of the coal matrix [-]

ε_{ij} : Strain tensor defined at the coal seam scale [-]

ϕ_c : Cleat porosity or macroporosity [-]

μ : Viscosity of fluid [cp]

ν, ν_3 : Horizontal and vertical Poisson ratios [-]

σ_{ij} : Total stress tensor defined at the coal seam scale [-]

ρ_b : Bulk molar density of the fluid [mol/L]

Units conversion

1 ft = 0.3048 m

1 psi = 6895 Pa

1 cp = 0.001 Pa.s

1476
 1477
 1478
 1479
 1480
 1481
 1482
 1483
 1484
 1485
 1486
 1487
 1488
 1489
 1490
 1491
 1492
 1493
 1494
 1495
 1496
 1497
 1498
 1499
 1500
 1501
 1502
 1503
 1504
 1505
 1506
 1507
 1508
 1509
 1510
 1511
 1512
 1513
 1514
 1515
 1516
 1517
 1518
 1519
 1520
 1521
 1522
 1523
 1524
 1525
 1526
 1527
 1528
 1529
 1530
 1531
 1532
 1533
 1534

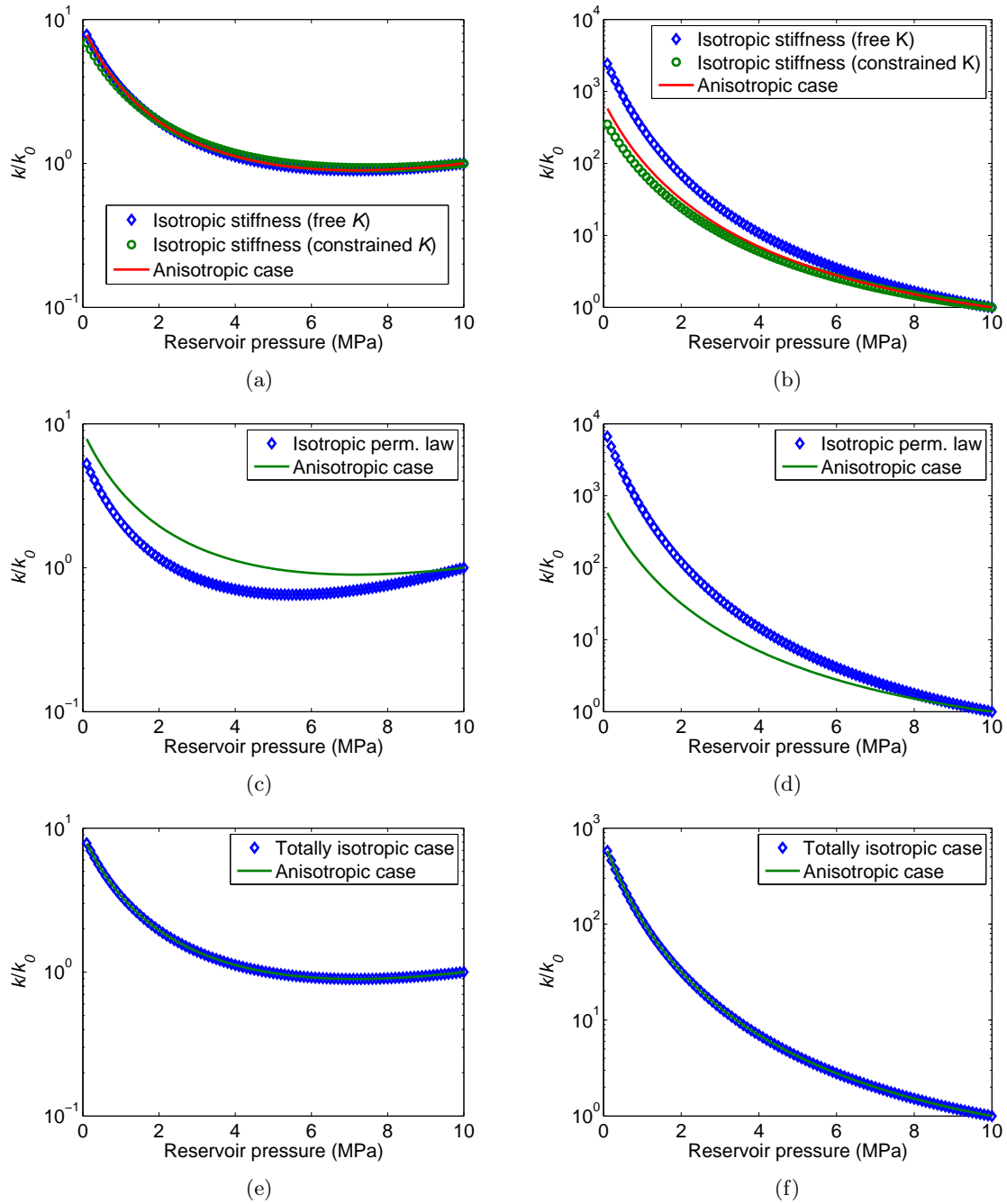


Figure 5: The k - P relationships in oedometric (left) and isochoric (right) conditions for the equivalent materials when disregarding the anisotropy of stiffness (a)(b), the anisotropy of permeability dependence on stresses (c)(d), and the anisotropy of both (e)(f).

1535
 1536
 1537
 1538
 1539
 1540
 1541
 1542
 1543
 1544
 1545
 1546
 1547
 1548
 1549
 1550
 1551
 1552
 1553
 1554
 1555
 1556
 1557
 1558
 1559
 1560
 1561
 1562
 1563
 1564
 1565
 1566
 1567
 1568
 1569
 1570
 1571
 1572
 1573
 1574
 1575
 1576
 1577
 1578
 1579
 1580
 1581
 1582
 1583
 1584
 1585
 1586
 1587
 1588
 1589
 1590
 1591
 1592
 1593

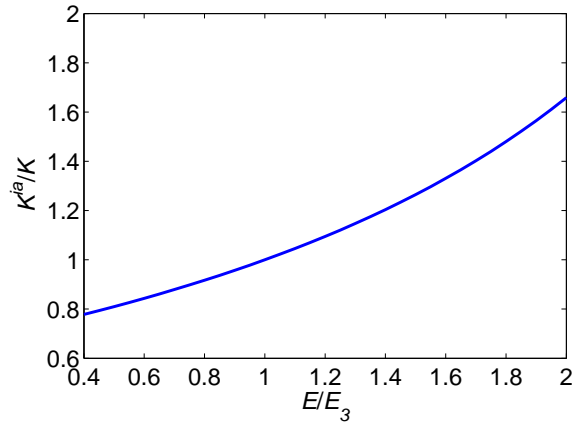


Figure 6: The mismatch in the bulk modulus when neglecting the anisotropy of stiffness using the free K method.

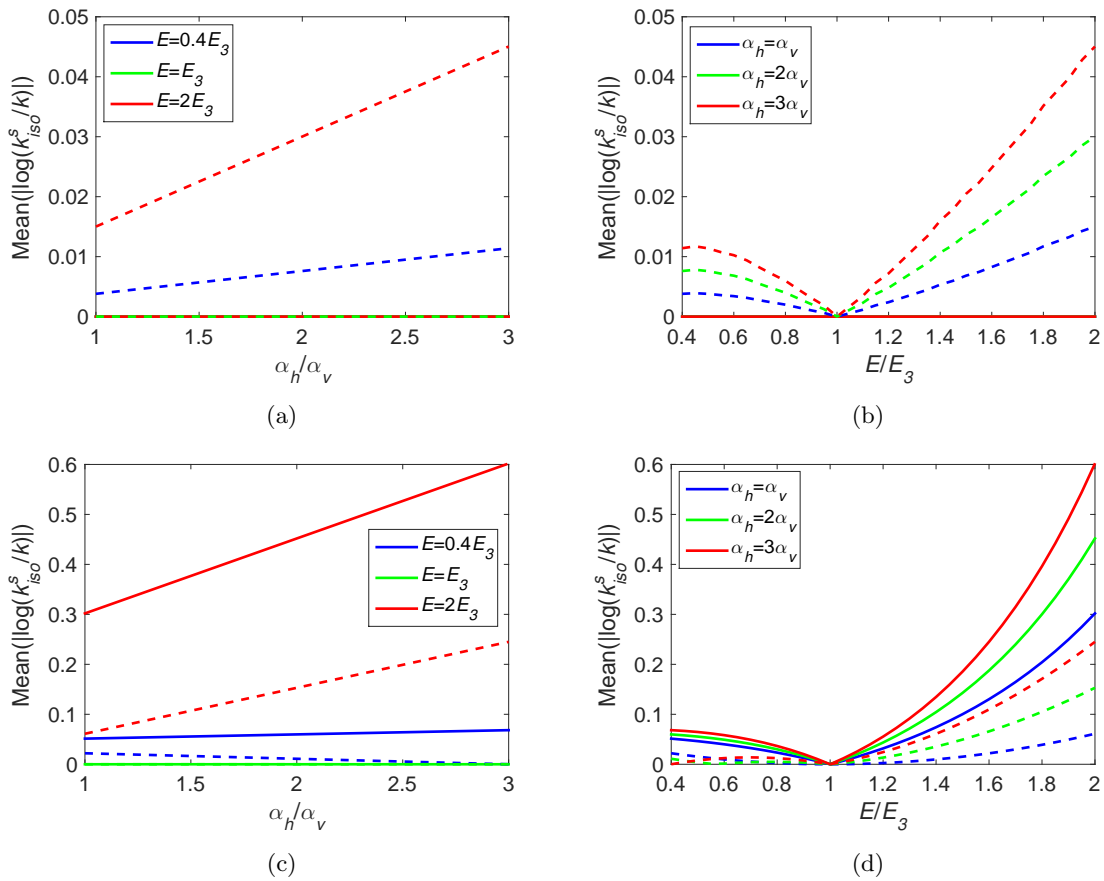


Figure 7: The errors on permeability introduced when disregarding the anisotropy of stiffness, depending on α_h/α_v (left) and E/E_3 (right) in oedometric (top) and isochoric (bottom) conditions (solid line: free K method, dashed line: constrained K method).

1594
1595
1596
1597
1598
1599
1600
1601
1602
1603
1604
1605
1606
1607
1608
1609
1610
1611
1612
1613
1614
1615
1616
1617
1618
1619
1620
1621
1622
1623
1624
1625
1626
1627
1628
1629
1630
1631
1632
1633
1634
1635
1636
1637
1638
1639
1640
1641
1642
1643
1644
1645
1646
1647
1648
1649
1650
1651
1652

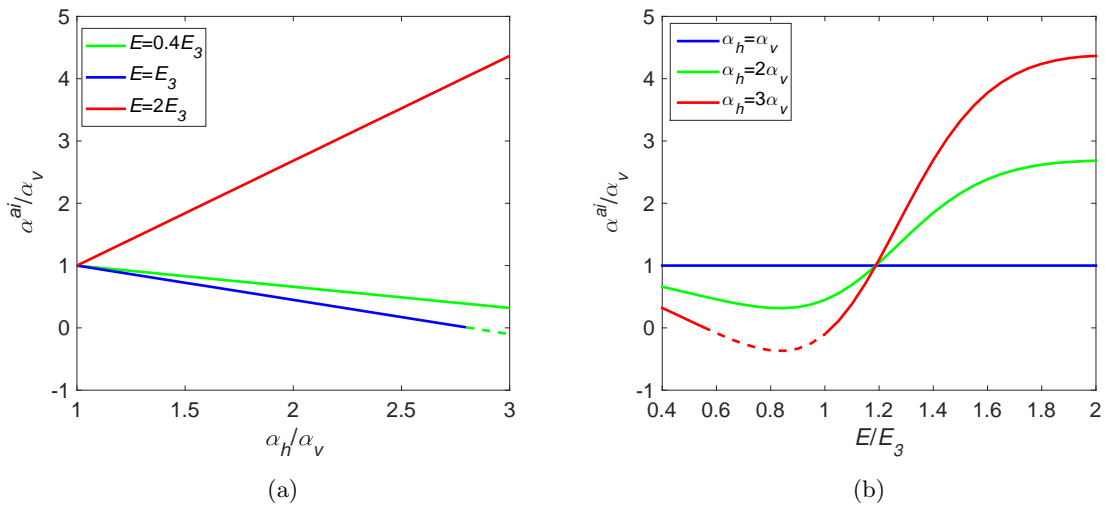


Figure 8: The assessed α^{ai} values in the case of neglecting the anisotropy of permeability dependence on stresses, depending on (a) α_h/α_v and (b) E/E_3 . The fittings provide sometimes negative α^{ai} values which are illustrated in dashed lines.

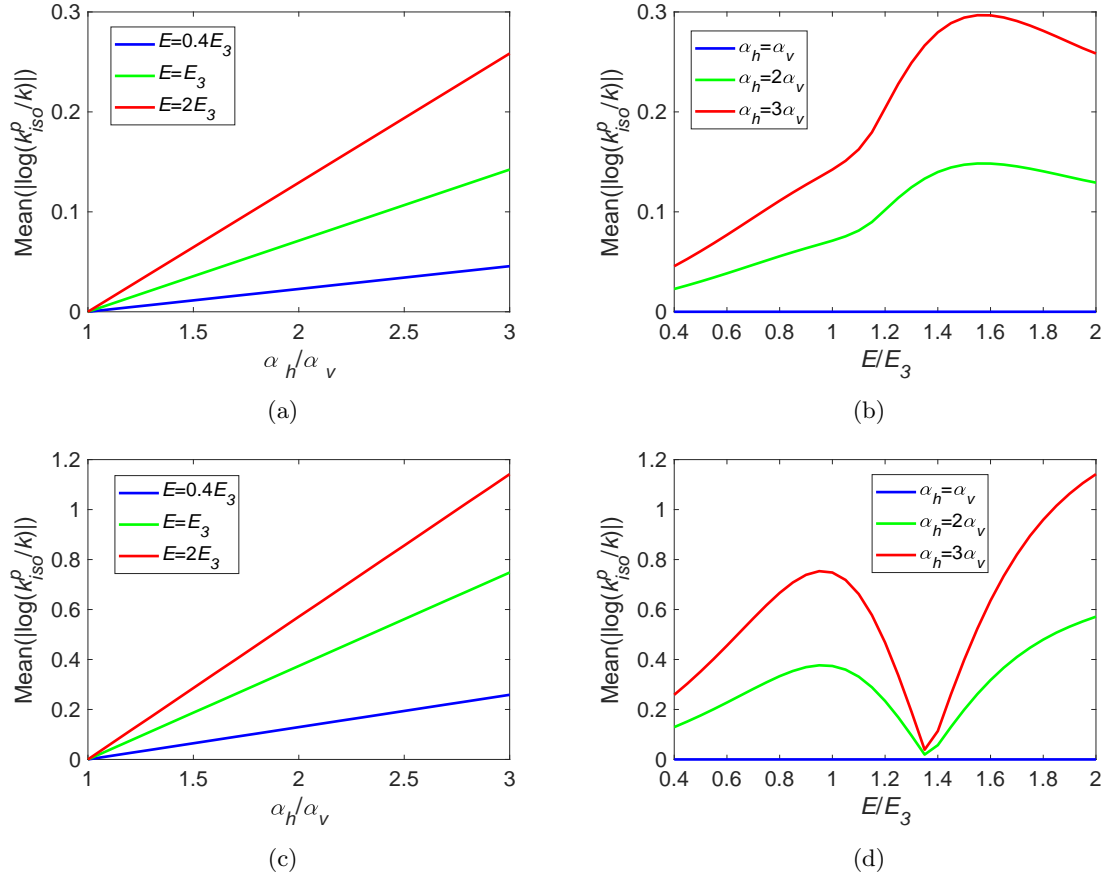


Figure 9: The errors on permeability introduced when disregarding the anisotropy of permeability dependence on stresses, depending on α_h/α_v (left) and E/E_3 (right) in oedometric (top) and isochoric (bottom) conditions.

1653
 1654
 1655
 1656
 1657
 1658
 1659
 1660
 1661
 1662
 1663
 1664
 1665
 1666
 1667
 1668
 1669
 1670
 1671
 1672
 1673
 1674
 1675
 1676
 1677
 1678
 1679
 1680
 1681
 1682
 1683
 1684
 1685
 1686
 1687
 1688
 1689
 1690
 1691
 1692
 1693
 1694
 1695
 1696
 1697
 1698
 1699
 1700
 1701
 1702
 1703
 1704
 1705
 1706
 1707
 1708
 1709
 1710
 1711

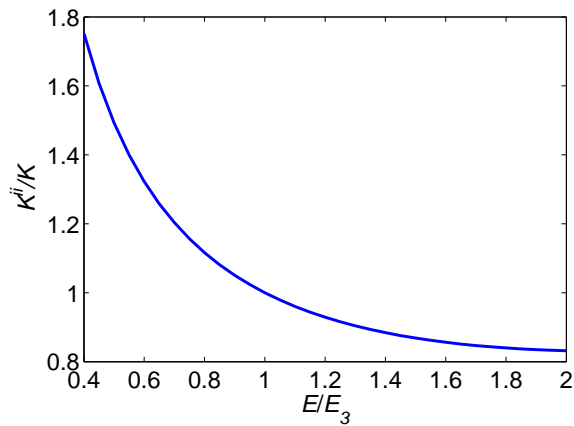


Figure 10: The mismatch in the bulk modulus for the totally isotropic case.

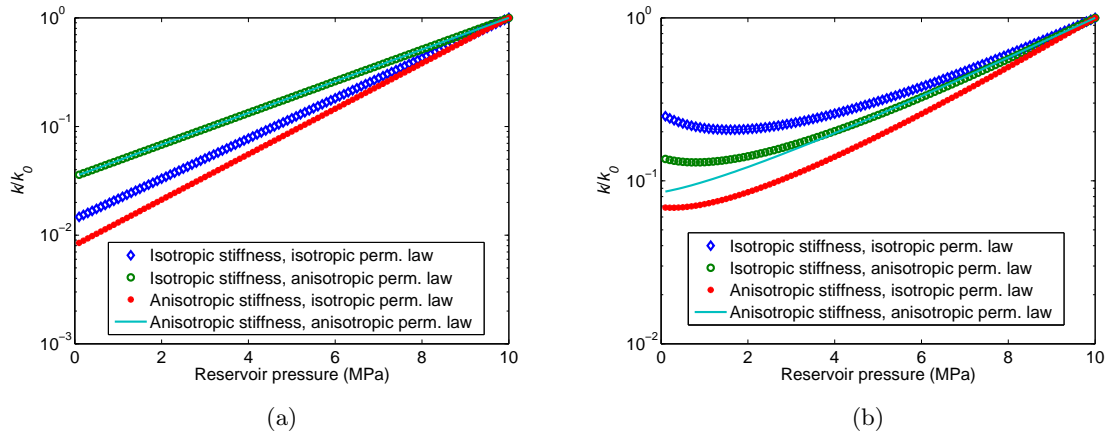


Figure 11: The k - P curves for the totally isotropic case in (a) free swelling (i.e., $\Delta\sigma_r = \Delta\sigma_a = 0$) and (b) inverse oedometric (i.e., $\Delta\sigma_r = 0, \Delta\varepsilon_a = 0$) conditions.

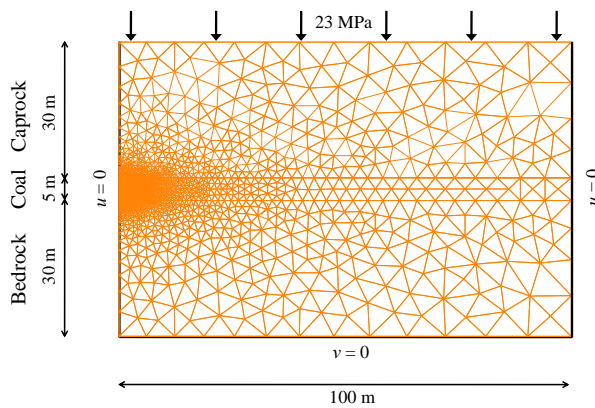


Figure 12: The model used for the reservoir simulation of methane recovery.

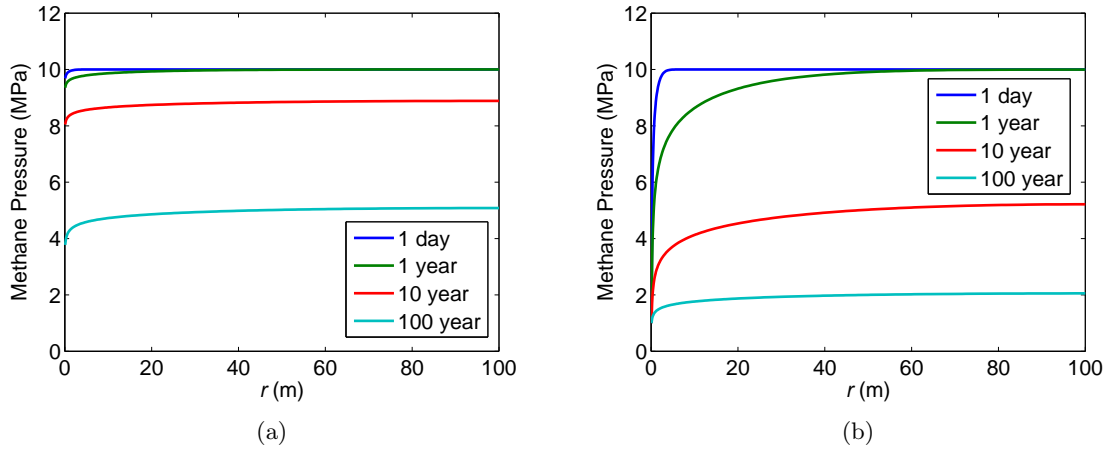


Figure 13: Methane pressure profiles at different times in the cases of constant flow (a) and of constant pressure (b) at wellbore from the reservoir simulation.

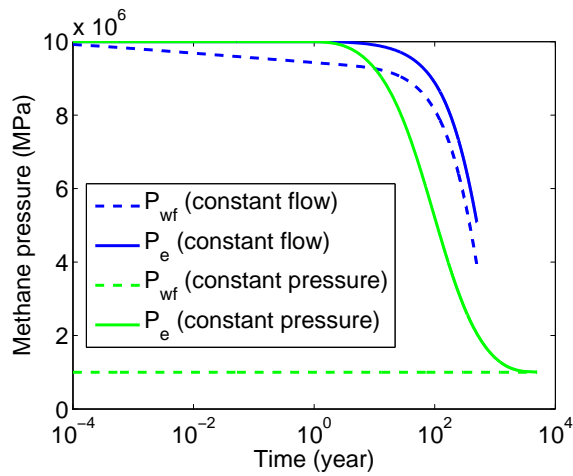


Figure 14: Evolution of borehole pressure (P_{wf}) and pressure at the outer boundary (P_e).

1771
1772
1773
1774
1775
1776
1777
1778
1779
1780
1781
1782
1783
1784
1785
1786
1787
1788
1789
1790
1791
1792
1793
1794
1795
1796
1797
1798
1799
1800
1801
1802
1803
1804
1805
1806
1807
1808
1809
1810
1811
1812
1813
1814
1815
1816
1817
1818
1819
1820
1821
1822
1823
1824
1825
1826
1827
1828
1829

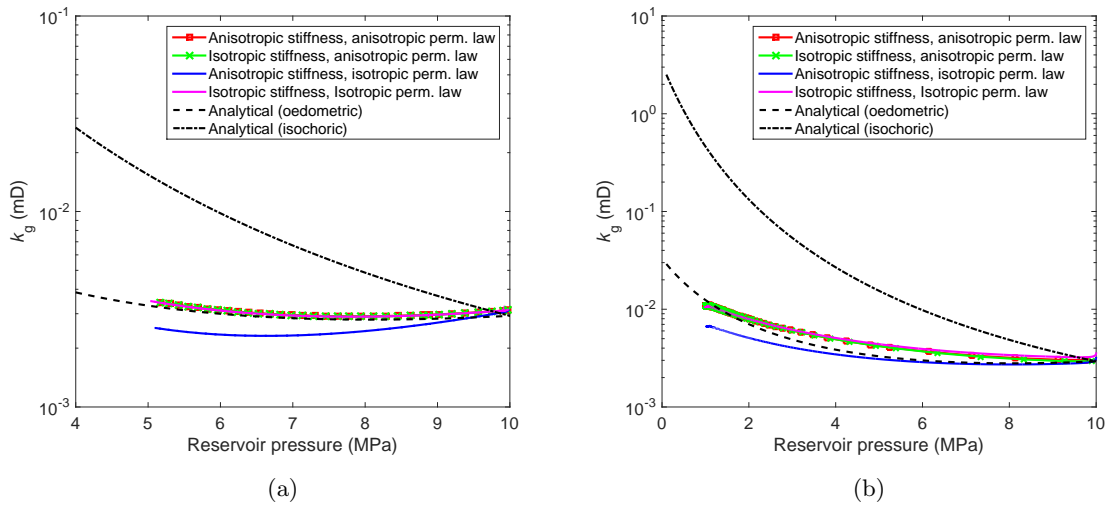


Figure 15: The k_g - P curves evaluated from the reservoir simulation in the cases of constant flow (a) and of constant pressure (b) at the wellbore.